

## **BISTATIC RCS PREDICTION FOR COMPLEX TARGETS USING MODIFIED CURRENT MARCHING TECHNIQUE**

**X. F. Li, Y. J. Xie, and R. Yang**

National Laboratory of Antennas and Microwave Technology  
Xidian University  
P. O. Box 223, Xi'an, Shaanxi 710071, P. R. China

**Abstract**—The improved high-frequency method for solving the bistatic scattering from electrically large conductive targets is presented in this paper. Since the previous physical optical methods overlooked the current impact of shadow zone and led to the increasing problems of the large angle bistatic calculation, the improved method is deduced by introducing the current marching technique into the conventional physical optical method. Combined with the graphical-electromagnetic computing method that extracted the illuminated and shadow facet in accordance with the direction of the incident sort iteration, one may calculate the bistatic radar cross-section of a conductive targets object. The numerical results show that this method is efficient and accurate.

### **1. INTRODUCTION**

With the stealth and anti-stealth technology development, the researchers have directed significant attention toward the targets of stealth in free space, especially the bistatic RCS Prediction for electrically large PEC targets. Radar development over the past 50 years has focused on two primary radar technologies: monostatic and bistatic. The distinction originates in the signal transmission and reception configuration. In the monostatic scenario, co-located antennas (or more typically the same antenna) transmit and receive RF energy, while in a bistatic situation the antennas are physically separated. Although most research and practical application have been in the monostatic domain [1], the bistatic condition offers several key

---

Corresponding author: X. F. Li (afeng4819@163.com).

benefits. Both object detection and identification can be significantly enhanced through utilization of the additional dimension provided by a bistatic geometry.

Some researchers try to combine the Method of Moment (MOM) to consider the bistatic scattering of the electrically large targets in free space, but it requires more mass storage memory, which results in lower processing speed and computational efficiency. Due to the above restrictions, iterative methods with extremely fast convergence (in just a few iterations) have recently been applied to bistatic RCS prediction. Finite Difference Time Domain (FDTD) [2], Current Marching Technique (CMT) [3], as the discrete space needs a huge number of grids and successive forward/backward calculations of the current demand for a longer time limit, do not apply to the bistatic prediction of electrically large conductive targets. The field marching technique [4] is obviously more accurate in large angle bistatic calculation, but it also has the paraxial limitations of the parabolic equation (PE) method. In particular, the high computational complexity has been introduced in the calculation of the three-dimensional scattering and in fact it is difficult to achieve results in less time.

Crispin, Goodrich and Siegel [5] have considered bistatic scattering at angles less than  $\pi$  and developed the “mono static-bistatic equivalence theorem”. Crispin et al. show the physical optics approximation with which the theorem is approximately true if the bistatic angle is considerably less than  $\pi$  radians, but it would lead to increasing problems in the large angle bistatic calculation. Some researchers use the bistatic scattering of polygon surface [6], for the methods overlooking the current impact of shadow zone and also leading to the increasing problems of the large angle bistatic calculation. The impact on current of the shadow region is small; however, in some applications the scattering of their contributions can not be ignored. Bistatic RCS computing has achieved initial results, but methods of testing are needed to be strong, particularly in the large angle bistatic cases lack an effective method of calculation.

In this paper, we present an improved high-frequency method for solving the bistatic scattering from electrically large conductive targets. For the previous physical optical (PO) methods overlooked the current impact of shadow zone and led to the increasing problems of the large angle bistatic calculation, the improved method is deduced by introducing the improved current marching technique into conventional PO method. Combined with the graphical-electromagnetic computing method that extracted the illuminated and shadow facet in accordance with the direction of the incident sort iteration, we can spend less

time calculating the bistatic radar cross-section of a conductive targets object (except for cavities, targets with cavities, FSS, dielectric or magnetic coating, etc).

In the next section, graphical processing that extracted the illuminated and shadow facet in accordance with the direction of the incident sort iteration and further formulated for improved high-frequency method is described. In Section 3, simulations and measurements for the electrically large conductive targets are given, and Section 4 contains conclusions.

## 2. THEORY

As shown in Fig. 1, consider an arbitrarily shaped object illuminated by a plane wave in the free space, surface  $S$  is assumed to represent a closed surface of target.

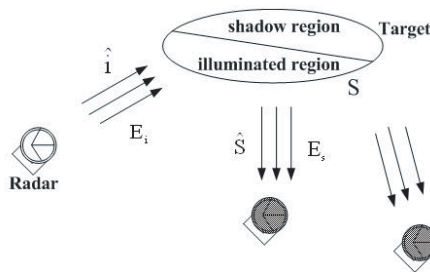


**Figure 1.** Geometry for bistatic scattering in the high-frequency region.

For the past high-frequency method overlooked the current impact of shadow region and led to the increasing problems of the large angle bistatic calculation, we included the improved current marching technique in our calculations by accounting for the currents that are induced on shadow facet. Thus, the term for the overall scattered field from a complex body may be written as:

Total scattered field = scattered fields from the illuminated facets + scattered fields from the shadow facets.

When calculating these fields one may proceed by using magnetic or electric field integral equation formulations. The following calculations are presented in terms of electric field formulations.

### 2.1. Bistatic Scattering in Illuminated Region

According to the high-frequency theory, we can get the accurate surface current by applying physical optics approximations over illuminated

surface in free space. Through the proper boundary conditions, the surface current can be represented as:

$$J \approx 2\hat{n} \times H_i \quad (1)$$

where  $\hat{n}$  is the inward surface unit normal;  $H_i$  is the polarization unit vectors for incident magnetic field.

To apply the far-field approximation, that is, the observation point is located far enough from the scattering object, the electric field integral equation [6–8] was reduced to the following expression:

$$E_s = jk\psi_0 \int_s \hat{s} \times \left[ \hat{n} \times \bar{E} - Z_0 \hat{s} \times (\hat{n} \times \bar{H}) \right] e^{jk\bar{r} \cdot (\vec{i} - \vec{s})} dS \quad (2)$$

where  $\varphi_0$  is  $\exp(-jkr)/r$ . According to the physical optics (PO) technique, Eq. (2) is reduced to the following expression for the scattered field of illuminated facet:

$$E_{sl} = \frac{jk \exp(-jkr) E_i}{2\pi r} \hat{s} \times \left[ \hat{s} \times (\hat{n} \times \hat{h}_i) \right] \int_{\Sigma} \exp \left[ jk (\hat{s} - \hat{i}) \cdot \bar{r}' \right] ds' \quad (3)$$

and we used the following notation:

$E_{sl}$  = scattered field due to the illuminated facet's surface

$K = 2\pi/\text{wavelength}$  of incident radiation

$\hat{e}_i, \hat{h}_i$  = polarization unit vectors for incident electric and magnetic fields

$\hat{i}, \hat{s}$  = incident and scattered propagation unit vectors.

Discrete computation of surface integral (3) leads to:

$$E_{sl} = \frac{jk \exp(-jkr) E_i}{2\pi r} \sum_{n=1}^N \hat{s} \times \left[ \hat{s} \times (\hat{n} \times \hat{h}_i) \right] \exp \left[ jk (\hat{s} - \hat{i}) \cdot \bar{r}' \right] \cdot \Delta S_n \quad (4)$$

The surface integral extends only over the region illuminated by the incident wave. It must be noted that (4) is correct only if a pixel radiates as an infinitesimal aperture, i.e., it is equivalent to the projection on the screen of a differential of surface much smaller than a wavelength.

## 2.2. Bistatic Scattering in Shadow Region

In the traditional high-frequency method [9–11], we often overlook the shadow of the side effects. The impact on current of the shadow region is small; however, in some applications the scattering

of their contributions can not be ignored. In this case, we use graphical-electromagnetic computing method [12] to compute the bistatic scattering of illuminated facets, then the shadow facets were calculated by improved current marching technique. Combined with their respective advantages, the improved method avoids spending a lot of memory and time solving the bistatic scattering of complex targets.

Current marching technique [3] solves the current of shadow facets by an iteration process that computes successive induced currents. These are marched forward and backward relative to the direction of the incident wave until convergence is obtained. They correspond to Gauss-Seidel iteration of the process, updating one point at a time. The unique solution of the dual surface integral equation is approached by forward/backward calculations of the current:

$$J_N(r) = 2n \times h_i + 2n \times \sum_{j=1}^N J(r'_j) \times \int_{s_j} \text{grad}_{r'}(G(r, r')) dS(r') \quad (5)$$

The forward is defined by applying these local operators repeatedly to points with increasing and decreasing ranges, respectively. It is defined inductively by

$$\begin{aligned} J(r_1) &= 2n_1 \times h_i + 2n_1 \times \sum_{j=1}^N J(r_j) \times \int_{s_j} \text{grad}_{r'}(G(r_j, r')) dS(r') \\ J(r_2) &= 2n_2 \times h_i + 2n_2 \times J(r_1) \times \int_{s_1} \text{grad}_{r'}(G(r_1, r')) dS(r') \\ &\quad + 2n_2 \times \sum_{j=2}^N J(r_j) \times \int_{s_j} \text{grad}_{r'}(G(r_j, r')) dS(r') \\ &\quad \vdots \\ J(r_i) &= 2n_i \times h_i + 2n_i \times \sum_{j=1}^{i-1} J(r_j) \times \int_{s_j} \text{grad}_{r'}(G(r_j, r')) dS(r') \\ &\quad + 2n_i \times \sum_{j=i}^N J(r_j) \times \int_{s_j} \text{grad}_{r'}(G(r_j, r')) dS(r') \\ &\quad \vdots \end{aligned} \quad (6)$$

$$\begin{aligned}
J(r_N) &= 2n_N \times h_i + 2n_N \times \sum_{j=1}^{N-1} J(r_j) \times \int_{s_j} \text{grad}_{r'}(G(r_j, r')) dS(r') \\
&\quad + 2n_N \times J(r_N) \times \int_{s_N} \text{grad}_{r'}(G(r_N, r')) dS(r')
\end{aligned}$$

We update the magnetic field and the current at successive ranges, replacing the current a given range by that induced by the new magnetic field values before that range and the old field values after that range. Similarly, backward operators is defined inductively by

$$\begin{aligned}
J(r_N) &= 2n \times h_i + 2n \times \sum_{j=1}^N J(r_j) \times \int_{s_j} \text{grad}_{r'}(G(r_j, r')) dS(r') \\
J(r_{N-1}) &= 2n_{N-1} \times h_i + 2n_{N-1} \times J(r_N) \times \int_{s_N} \text{grad}_{r'}(G(r_j, r')) dS(r') \\
&\quad + 2n_{N-1} \times \sum_{j=1}^{N-1} J(r_j) \times \int_{s_j} \text{grad}_{r'}(G(r_j, r')) dS(r') \\
&\quad \vdots \\
J(r_i) &= 2n_i \times h_i + 2n_i \times \sum_{j=i+1}^N J(r_j) \times \int_{s_j} \text{grad}_{r'}(G(r_j, r')) dS(r') \\
&\quad + 2n_i \times \sum_{j=1}^i J(r_j) \times \int_{s_j} \text{grad}_{r'}(G(r_j, r')) dS(r') \\
&\quad \vdots \\
J(r_1) &= 2n_1 \times h_i + 2n_1 \times \sum_{j=1}^{N-1} J(r_j) \times \int_{s_j} \text{grad}_{r'}(G(r_j, r')) dS(r')
\end{aligned} \tag{7}$$

In the high frequency area, we notice that the current of illuminated region is mainly induced by the plane-wave radiation. The shadow, which occurs on the opposite side of the object from the energy source, describes a region in which the electromagnetic fields are very small, implying that the currents induced in the object by the incident wave reradiate a secondary electromagnetic wave that cancels the incident wave in the shadow region. Combined with the incentive items

in illuminated region, the current of shadow zone is mainly affected by the mutual coupling of each facets, so we discovered the coupling term of CMT and applied it to bistatic scattering of electrically large conductive targets in shadow region.

Working with Cartesian coordinates, we assume that the incident field propagates along the positive direction. We now use the direction of the incident as our splitting direction for the forward/backward iteration. From now on, we assume our grid points are ordered in increasing ranges. The coupled current of shadow facets can be expressed as:

$$J(r) = 2n \times \sum_{j=1}^N J(r_j) \times \int_{s_j} \text{grad}_{r'} (G(r, r')) dS(r') \quad (8)$$

And substitute (8) into the scattered field (2) due to the shadow facets, which lead to the scattered electric field  $E_{sd}$ .

Then the complex bistatic RCS due to scattering from  $N$  illuminated facets and  $M$  shadow facets is calculated as Eq. (9):

$$\sigma = 4\pi \lim_{R \rightarrow \infty} R^2 \frac{\left| \sum_{n=1}^N (E_{st} \cdot \hat{e}_r)_n + \sum_{m=1}^M (E_{sd} \cdot \hat{e}_r)_m \right|^2}{|E_o|^2} \quad (9)$$

Here  $R$  is the position vector for the facet's reference vertex with respect to the global coordinate system.

Since the required number of iterations does not depend on object size, execution times are of the order of  $N^2$ , which means that relatively large objects are still tractable on a desktop computer. In order to consider the efficiency and need, we consider the first iteration temporarily. Even though the iteration was limited, interesting results are obtained with a single forward iteration. The results have been greatly improved.

### 2.3. Graphical Processing in Real-time

GRECO method was introduced by Rius in 1993 [12]. It can be integrated with CAD geometric modeling package and high-frequency theory for RCS prediction. By the hardware graphics accelerator, hidden surfaces of the image have been previously removed.

In this paper, the current marching technique is introduced into the conventional physical optical method to consider the current impact of shadow region. Meanwhile, the bistatic RCS of illuminated region is calculated with graphical electromagnetic computing method.

When an opaque object is illuminated by an electromagnetic wave, a shadow is produced if the object's dimensions are larger than a wavelength. As shown in Fig. 2, to the fixed screen, the calculation complexity is not varied with the complexity and dimension of targets. The targets are rebuilt by displaying lists technology of OpenGL and hidden surfaces of the image have been previously removed by the hardware graphics accelerator. Then we make use of the resolution to disperse the curve face into pixels that satisfy the requirement of the electromagnetic calculation. Meanwhile, the scene is rendered using the Phong local illumination model [13, 14]. Rotating through the coordinates of the matrix, the unit normal of shadow facets could be obtained by the same way.

The current marching technique is approached by successive forward/backward calculations of the current. From now on, as shown

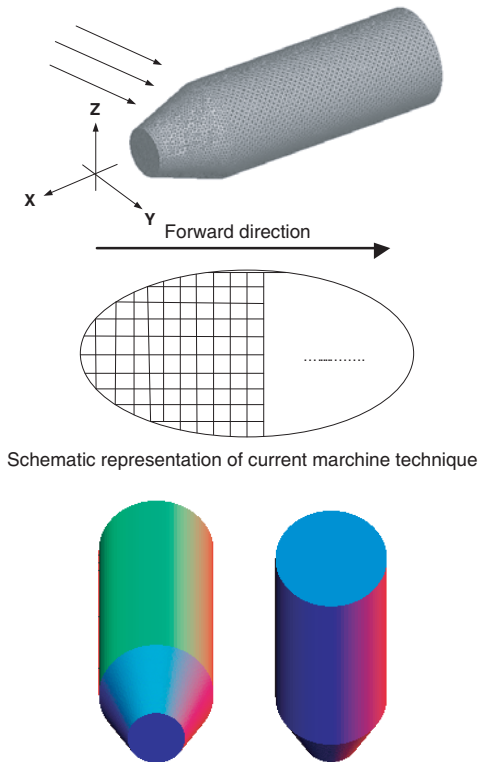


**Figure 2.** Schematic representation of graphical electromagnetic computing method in the illuminated and shadow region.

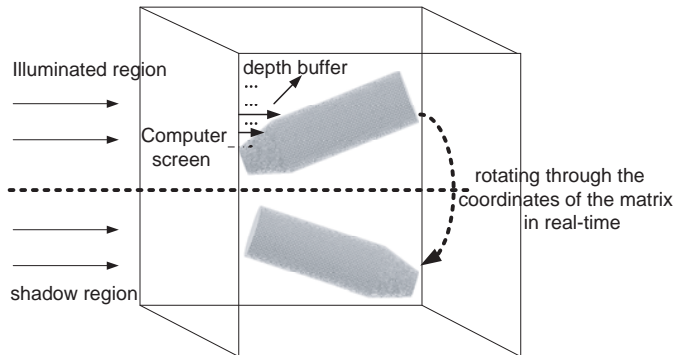


**Figure 3.** The process of the pixels are ordered with increasing ranges in the direction of the incident wave in the illuminated and shadow region.

in Fig. 3, the illuminated and shadow facets need to be extracted in accordance with the depth buffer in real-time, and the pixels of whole targets are ordered with increasing ranges in the direction of the incident wave.

The depth buffer is a buffer with the same width and height as your render target. This buffer records the depth of each pixel that is rendered. When a pixel is rendered a second time such as when one object is rendered behind another the depth buffer will keep either the previous depth value, or replace it with the depth value for the second pixel. Which depth is preserved and which depth is discarded depend on the depth function you select. Depth values that are less than or equal to the current value are preserved. Any value greater than the current depth value is discarded. This is called the depth test. The depth test occurs every time a pixel is rendered. When a pixel passes the depth test, its color is written to the render target and its depth is written to the depth buffer.

Through using the above method, the geometric information of each pixel of the whole target was obtained in real-time, and it greatly reduces the computing time which change the direction of the incident sort iteration.

### 3. NUMERICAL RESULTS

To ensure correlation with computations, special attention was given to the accuracy of model construction. The convention method overlooked the current impact of shadow zone and led to the

increasing problems in horizontal polarization and vertical polarization calculation. The comparison of two polarizations is important. For the symmetric goal, we adopt the vertical polarization as a standard, and the comparison result has a smaller difference. Illustrations of the verification work are presented in the following sections.

We first look at regulation bodies for which the improved high-frequency algorithm is correct. Perfectly conducting spheres provide a good test of the method since theoretical solutions in the form of fast multipole algorithm (FMM) are available for comparison. Fig. 4 shows the RCS results obtained with the improved method (GRECO + CMT). For comparison, the conventional GRECO solution is also shown. The conventional method does not give as good an approximation as fast multipole algorithm, which is understandable since it overlooked the current impact of shadow zone and led to the increasing problems of the large angle bistatic calculation.

From Fig. 5, we can see that in the large angle bistatic calculation between  $-180^\circ$  to  $-50^\circ$  and  $180^\circ$  to  $50^\circ$ , the convention method has a large error. The flashes due to the supporting tower were about 5–10 dBsm. And the accuracy limit is reached after the current marching technique was introduced into the conventional physical optical method, and the results corresponds very well to the theory.

As the frequency increases, the number of azimuthal modes required increases, and the FMM becomes less efficient. Although the conventional GRECO method needs less time, it has a larger error. Numerical experiments have revealed that the improved method becomes faster than the FMM solution. The improved method avoids spending a lot of memory and time solving the bistatic scattering of complex targets. Meanwhile, it has high accuracy.

As a further demonstration of the model utility, we present

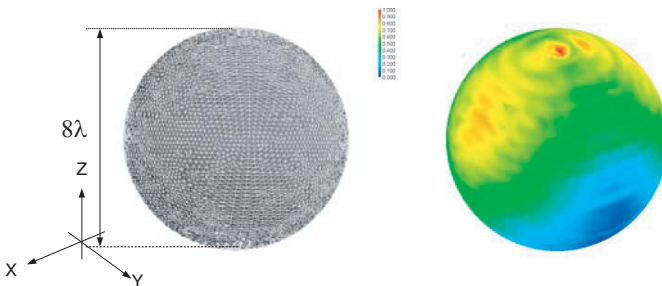


**Figure 4.** Induced normalised electric current on the surface of the sphere, frequency 10 GHz, vertical polarization, at a incident angle of  $\theta_i = 0$ ,  $\varphi_i = 0$ .

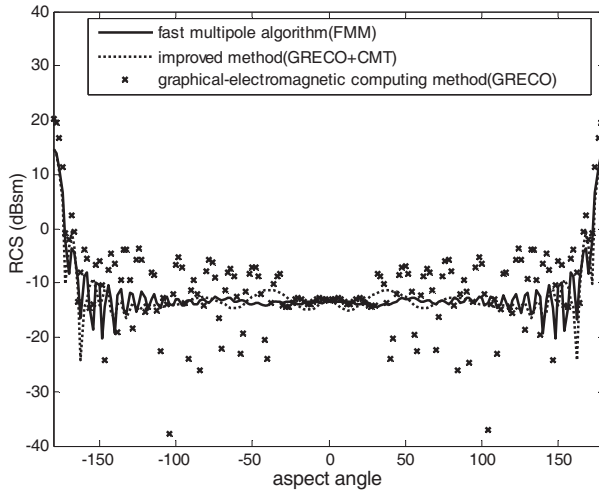


**Figure 5.** Bistatic RCS of sphere, frequency 10 GHz, vertical polarization, at a incident angle of  $\theta_i = 0$ ,  $\varphi_i = 0$ .

**Table 1.** Bistatic RCS of sphere. The comparison of there method (memory storage, CPU time).

The method	Memory storage	CPU time
Fast multipole algorithm (FMM)	148 M	57 min
improved method (GRECO + CMT)	55 M	5 min
Graphical electromagnetic computing method (GRECO)	79 M	25 min

example induced electric current on the surface of the column, for vertical polarization, at an incident angle of  $\theta_i = 30$ ,  $\varphi_i = 0$ . As shown in Fig. 6, the impact on current of the shadow region is small; however, in some applications the scattering of their contributions cannot be ignored.

We consider that the current of illuminated region is mainly induced by the plane-wave radiation. The shadow, which occurs on the opposite side of the object from the energy source, describes a region in which the electromagnetic fields are very small, implying that the currents induced in the object by the incident wave reradiate

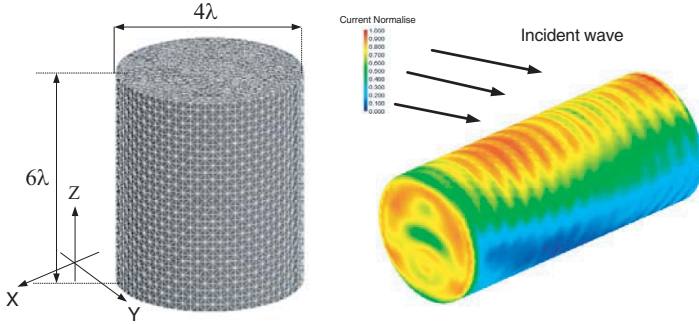


**Figure 6.** Induced normalised electric current on the surface of the Column, frequency 10 GHz, vertical polarization, at a incident angle of  $\theta_i = 30$ ,  $\varphi_i = 0$ .

**Table 2.** Bistatic RCS of Cone-Column. The comparison of there method (memory storage, CPU time).

The method	Memory storage	CPU time
Fast multipole algorithm (FMM)	132 M	25 min
improved method (GRECO + CMT)	79 M	6 min
Graphical electromagnetic computing method (GRECO)	85 M	15 min

a secondary electromagnetic wave that cancels the incident wave in the shadow region. Combined with the incentive items in illuminated region, the current of shadow zone is mainly affected by the mutual coupling of each facets. The improved method avoids spending a lot of memory and time solving the bistatic scattering of complex targets.

Figure 7 shows the bistatic RCS of column with a  $30^\circ$  illumination and a further comparison between the improved theory and the fast multipole algorithm. It provides a challenging test, as they do not have special point of view. It is interesting to note that the results are in better agreement with FMM results, and it is far beyond the speed of operation to other methods.

Finally, we treat the case of the Cone-Column with a  $60^\circ$  illumination shown in Fig. 8. This produced very satisfactory results.

Fig. 9 shows that the contributions of shadow facets cannot be ignored. It indicates the excellent agreement of improved high-frequency predictions for a cone-column compared to range

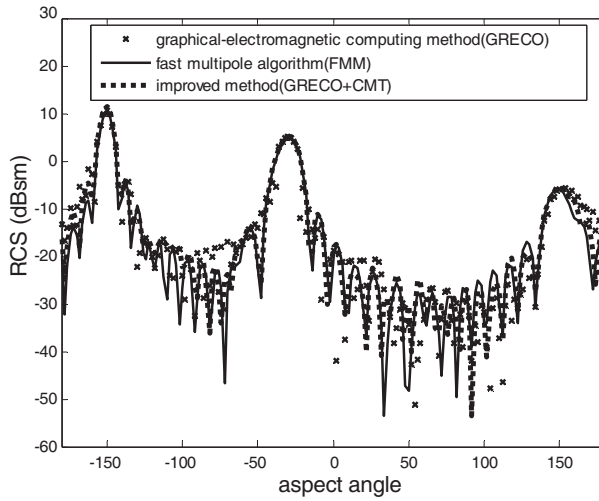


**Figure 7.** Bistatic RCS of Column, frequency 10 GHz, vertical polarization.

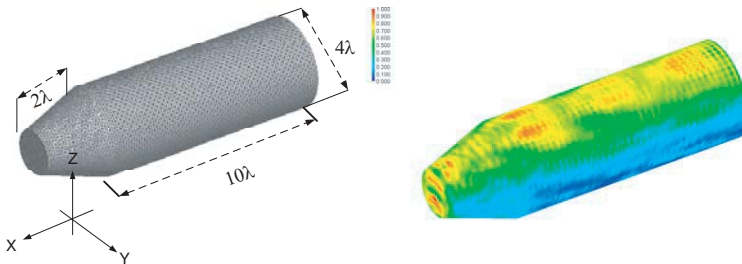


**Figure 8.** Induced normalised electric current on the surface of the Cone-Column, frequency 10 GHz, vertical polarization, at a incident angle of  $\theta_i = 60$ ,  $\varphi_i = 0$ .

measurements as well as a FMM result. Keeping in mind the interferences of the tower flashes with the target’s return, the overall agreement is very good, except for the slightly higher fluctuations around  $150^\circ$ . It was found that iterative methods may diminish the phase correlation in certain situations.

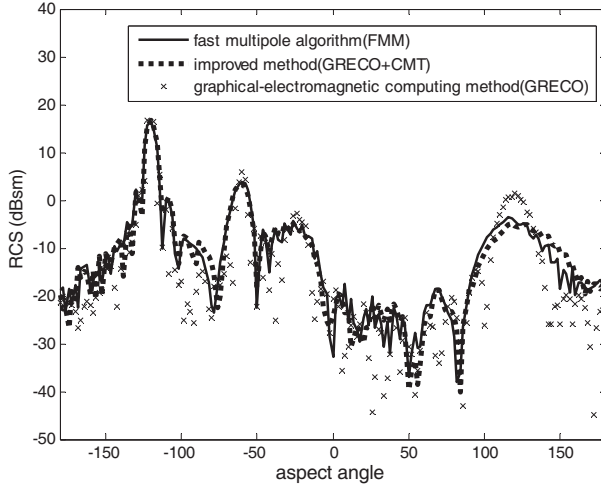


**Figure 9.** Bistatic RCS of Cone-Column, frequency 10 GHz, vertical polarization.

**Table 3.** Bistatic RCS of Cone-Column. The comparison of there method (memory storage, CPU time).

The method	Memory storage	CPU time
Fast multipole algorithm (FMM)	472 M	85 min
improved method (GRECO + CMT)	85 M	9 min
Graphical electromagnetic computing method (GRECO)	85 M	36 min

#### 4. CONCLUSION

In this paper, we have presented an accurate and efficient approach for calculating the bistatic RCS prediction for electrically large PEC targets. In order to consider current impact of shadow zone, the current marching technique was introduced into the conventional high-frequency method. Combined with the graphical-electromagnetic computing method that extracted the illuminated and shadow facet in accordance with the direction of the incident sort iteration, one may calculate the bistatic radar cross section of a conductive targets object.

The initial results compare well with theory and other method. Due to the graphical-electromagnetic computing method, the graphics

data could be processed in real-time, and it is possible to have a trade off between time and memory requirements and to treat electrically large objects on personal computers.

## ACKNOWLEDGMENT

The project was supported by National Natural Science Foundation of China.

## REFERENCES

1. Gustafsson, M., "RCS reduction of integrated antenna arrays with resistive sheets," *Journal of Electromagnetic Waves and Applications*, Vol. 20, No. 1, 27–40, 2006.
2. Wang, M. Y., J. Xu, J. Wu, Y. Yan, and H. L. Li, "FDTD study no scattering of metallic column covered by double negative metamaterial," *Journal of Electromagnetic Waves and Applications*, Vol. 21, 1905–1914, 2007.
3. Zaporozhets, A. A. and M. F. Levy, "Current marching technique for electromagnetic scattering computations," *IEEE Trans. on Antennas and Propag.*, Vol. 47, No. 6, 1016–1024, 1999.
4. Zaporozhets, A. A. and M. F. Levy, "Bistatic RCS calculations with the vector parabolic equation method," *IEEE Trans. on Antennas and Propag.*, Vol. 47, No. 11, 1688–1696, 1999.
5. Crispin, J. W., R. F. Goodrich, and K. M. Siegel, "A theoretical method for the calculation of radar cross section of aircraft and missiles," Report No. 2591-1-H, University of Michigan, 1959.
6. Hatamzadeh-Varmazyar, S. and M. Naser-Moghadasi, "An integral equation modeling of electromagnetic scattering from the surfaces of arbitrary resistance distribution," *Progress In Electromagnetics Research B*, Vol. 3, 157–172, 2008 .
7. Li, Y., Y. Liu, and S. Gong, "Microstrip antenna using ground-cut slots and miniaturization techniques with low RCS," *Progress In Electromagnetics Research Letters*, Vol. 1, 211–220, 2008.
8. Valagiannopoulos, C. A., "Closed-form solution to the scattering of a skew strip field by metallic pin in a slab," *Progress In Electromagnetics Research*, PIER 79, 1–21, 2008.
9. Ross, R. A., "Bistatic scattering from rectangular plates," *Journal of Electromagnetic Waves and Applications*, Vol. 19, 1111–1124, 2005.
10. Zheng, J. H., Y. Liu, and S. X. Gong, "Aperture coupled

- microstrip antenna with low RCS,” *Progress In Electromagnetics Research Letters*, Vol. 3, 61–68, 2008
11. Mishra, M. and N. Gupta, “Monte carlo integration technique for the analysis of electromagnetic scattering from conducting surfaces,” *Progress In Electromagnetics Research*, PIER 79, 91–106, 2008.
  12. Rius, J. M., M. Ferrando, and L. Jofre, “High-frequency RCS of complex radar targets in real-time,” *IEEE Antennas and Propag.*, Vol. 41, No. 9, 1308–1460, 1993.
  13. Li, X. F., Y. J. Xie, P. Wang, and T. M. Yang, “High-frequency method for scattering from electrically large conductive targets in half-space,” *IEEE Antennas and Wireless Propagation Letters*, Vol. 6, 259–262, 2007.
  14. Li, X., Y. Xie, and R. Yang, “High-frequency method for scattering from coated targets with electrically large size in half space,” *Microwaves, Antennas & Propagation*, Vol. 3, Issue 2, 181–186, 2008.